IEEE Access
Multidisciplinary : Rapid Review : Open Access Journal

Received March 13, 2019, accepted March 31, 2019, date of publication April 3, 2019, date of current version April 19, 2019.

Digital Object Identifier 10.1109/ACCESS.2019.2909172

A Frequency-Reconfigurable Antenna With 1-mm Nonground Portion for Metal-Frame and Full-Display Screen Handset Applications Using Mode Control Method

CHONG-ZHI HAN[1], SHU-MIN LIAO[1], KAI-DONG HONG[1], GUAN-LONG HUANG[1], (Senior Member, IEEE), TAO YUAN[1,2], WONBIN HONG[3], (Senior Member, IEEE), AND CHOW-YEN-DESMOND SIM[4], (Senior Member, IEEE)

[1]Guangdong Provincial Mobile Terminal Microwave and Millimeter-Wave Antenna Engineering Research Center, College of Information Engineering, Shenzhen University, Shenzhen 518060, China
[2]ATR National Key Laboratory of Defense Technology, College of Information Engineering, Shenzhen University, Shenzhen 518060, China
[3]Pohang University of Science and Technology, Pohang 37673, South Korea
[4]Department of Electrical Engineering, Feng Chia University, Taichung 40724, Taiwan

Corresponding authors: Guan-Long Huang (guanlong.huang@szu.edu.cn) and Tao Yuan (yuantao@szu.edu.cn)

This work was supported in part by the Shenzhen Science and Technology under Grant JCYJ20180305124721920, in part by the National Natural Science Foundation of China under Grant 61801300, and in part by the State Key Laboratory of Millimeter Waves under Grant K201932.

ABSTRACT A frequency-reconfigurable antenna featuring four integrated switches for metal-frame and full-display screen handset applications is proposed in this paper. To achieve full-display aesthetics, the nonground portion of the proposed antenna is reduced to only 1 mm, making it impossible to formulate additional parasitic strips to enhance the bandwidth and radiation efficiency of the antenna. Four switches are employed in conjunction with the devised antenna to excite five resonant modes using the mode control method (MCM) to operate from 699 to 960 MHz and from 1710 to 2690 MHz. The proposed antenna is designed by employing several peripheral metallic components, such as steel sheet, USB, speaker box, and full-display screen into consideration, which enables the overall structure to be much closer to a practical smartphone environment. A prototype was fabricated and measured. The experimental results confirm that the proposed antenna features radiation efficiency from 30% to 55% for metal-frame and full-display screen handset applications.

INDEX TERMS Frequency-reconfigurable, full-display screen, metal-frame, nonground portion, switches.

I. INTRODUCTION

Handset antennas have triggered much attention amid the proliferation of multiband wireless wide area network/long-term evolution (WWAN/LTE) for mobile communication [1]. Hence, multiband characteristic has been one of the most essential features for handset antennas during their research and development (R&D) process [2]. Several methods have been extensively studied to achieve wide operating bandwidth, in which applying appropriate matching network is a good way to enhance the bandwidth [3]–[8]. A high-pass matching network has been investigated in [4] to widen the higher frequency bandwidth to cover the LTE middle/high bands (1710 MHz-2690 MHz). For the antenna's lower band shown in [5], an additional resonant mode can be generated by adding a high-pass matching circuit in the antenna's feeding portion. In addition, parasitic elements/strips would also help antennas to generate more resonant modes, which results in an enhancement of antenna bandwidth [9]–[11]. A stair-like ground branch has been adopted to generate the higher resonant mode for LTE 2300/LTE 2500 [9]. Two parasitic grounded strips have also been used to provide

The associate editor coordinating the review of this manuscript and approving it for publication was Mingchun Tang.

monopole modes for the antenna shown in [10], which can cover the higher bandwidth of LTE. Nevertheless, the aforementioned methods are mainly suitable for handset antenna with sufficient nonground portion (or called metal clearance in some literatures) since a desired wide bandwidth of a single resonant mode requires a lower Q (antenna quality factor) value, which is usually corresponding to a relatively larger nonground portion. Moreover, the parasitic branches/strips have to occupy certain nonground portion to introduce extra resonant modes [12]. From this point of view, the requirement of 1-mm nonground portion for a handset antenna with full-display screen is insufficient to simultaneously operate in both the lower and the higher bands for WWAN/LTE mobile communication. However, by using another method of widening the operating bandwidth, reconfigurable techniques have been proven to be a more practicable approach in achieving wider impedance bandwidth [13], [14]. A reconfigurable antenna using two PIN diodes is reported for quad-band (GSM900/GSM1800/GSM1900/UMTS) mobile handset applications [13]. The proposed structure operates in both the PIFA and loop mode by adjusting the ON/OFF states of two PIN diodes. In particular, the two PIN diodes are placed on the radiating element of the antenna structure. The research seems to be a promising design, nevertheless, only a part of the lower bands (GSM900) can be covered. Another LTE smartphone antenna design covering a wide bandwidth of 698 MHz-960 MHz and 1710 MHz-2690 MHz has been proposed in [14], utilizing varactor diodes soldered between the open slots to adjust the radiation frequency of lower bands. Although the lower bandwidth of 698 MHz-960 MHz can be achieved, the nonground portion of the antenna is as large as 7 mm.

As one can presume from the aforementioned studies, it is extremely challenging to accomplish antenna designs in a relative narrow space (nonground portion) while adhering to the handsets' development trends towards multifunctionality and miniaturization. Furthermore, handsets/smartphones with metal-frame/metal-rim can further shrink the nonground portion of the handset antennas together with other peripheral metallic components such as USB, speaker box, and steel sheet. Thus, undesired electromagnetic coupling from these components would restrict the freedom of the antenna design. On the other hand, to satisfy the consumers' requirements, handsets design with metal-frame/metal-rim and full-display screen features are set to be the first priority, because it can keep the mechanical strength and aesthetic appearance simultaneously. Hence, designing handset antennas with metal-frame/metal-rim and full-display screen, together with other metallic components taken into consideration, is extremely important for mobile industrial application. Several handset antennas for metal-frame/metal-rim application due to its fantastic appearance and better robustness have been studied in [15]–[18]. A mobile phone antenna with full metal casing is proposed with 6 mm long nonground portion allocated on bottom edge of the system circuit board [15]. Good impendence matching is obtained across the frequency bands of 824 MHz-960 MHz and 1710 MHz-2690 MHz. Another compact multimode monopole antenna for metal-rimmed mobile phone is proposed in [18], which occupies an area of 60×58 mm^2 on a 120×60 mm^2 system circuit board. The metal-frame/rimmed handset antennas presented in [15]–[19] have a nonground portion ranging from 7 mm to 2 mm.

In this paper, a frequency-reconfigurable handset antenna with metal-frame and full-display screen architecture is proposed to cover the 699 MHz-960 MHz (GSM/LTE) and 1710 MHz-2690 MHz (DCS/PCS/UMTS/LTE) operating bands. It is noteworthy that the nonground portion of the proposed antenna is just 1 mm. The antenna structure proposed in this work also takes peripheral metallic components such as speaker box, USB, steel sheet and full-display screen into consideration during the design process. Four switches with nine states are utilized to offset the limited bandwidth from one single resonant state. As such practical design environment is seldom mentioned by other research works, the main objective of this work is to propose a practical approach to develop a frequency-reconfigurable handset antenna that can meet the 1-mm nonground portion requirement in a metal-frame/rimmed and full-display screen handset environment with desirable performances, while maintaining its appearance and robustness.

II. ANTENNA DESIGN IN HANDSET ENVIRONMENT

Fig. 1 shows the configuration of the proposed antenna with surrounding metallic components. An explosion-view of the proposed antenna is demonstrated in Fig. 1(a), from which three distinct layers of the structure can be observed. A screen, a steel sheet and a main board of the handset are integrated together from top to bottom layer to form the whole structure of the handset. Accordingly, three kinds of materials are employed in this work in order to evaluate the performance of the handset antenna more precisely: (1) the yellow color is copper, involved in the metal-frame of the handset, the steel sheet, the main board, the USB, the speaker box and the screws; (2) the purple one represents the screen of the handset, whose material is glass with permittivity of $\varepsilon_r = 4.82$ and loss-tangent $\tan\delta = 0.0054$; (3) the cyan one indicates the dielectric material of Acrylonitrile Butadiene Styrene plastic (ABS) with $\varepsilon_r = 2.8$ and $\tan\delta = 0.045$.

In Fig. 1(a) and (b), four switches will be placed at locations denoted as points ①, ②, ③ and ④. Here, point ① is the feeding part, where the switch added in this place can adjust the feeding network to different states. The other three switches placed at point ② , ③ and ④ can be considered as parallel loading. The detailed working principle of the four switches will be discussed in next section.

The main board and other metallic components that would affect the antenna performance are also described in Fig. 1(b). The width of the metal-frame is W. The 1-mm opening (G) is cut on the left and right side of the metal-frame. L and L_1-L_5 indicate the various distances between the main board and along the top metal-frame. To achieve a better view of the handset structure, another layer of the steel sheet is depicted

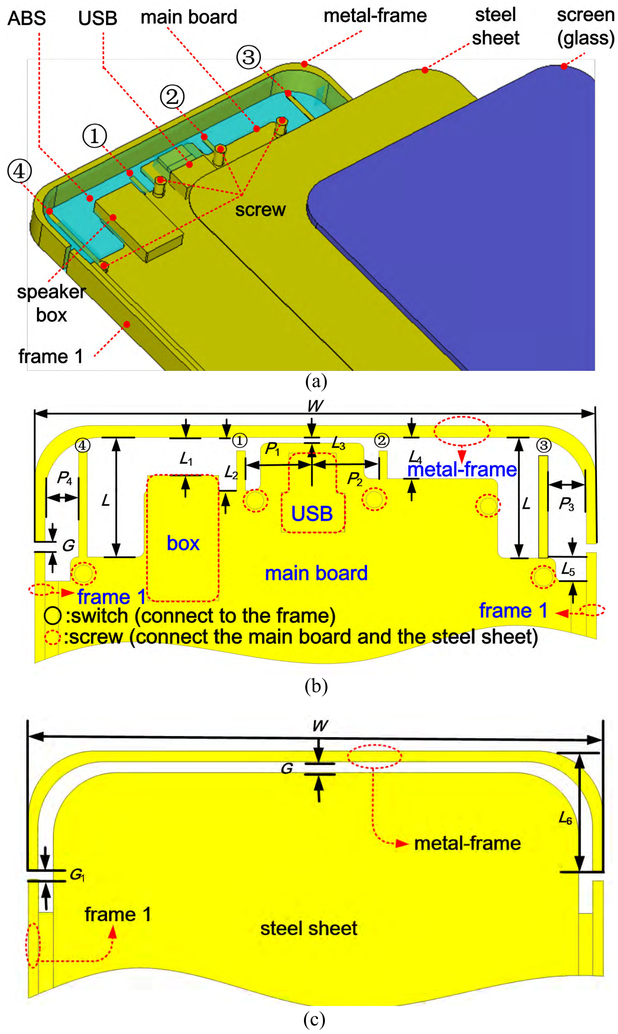

FIGURE 1. Geometry of the proposed antenna in the handset environment with peripheral metal components. (a) Explosion-view. (b) Bottom-view. (c) Top-view.

in Fig. 1(c). Four screws are embedded to connect the main board and the steel sheet, as all the large area of metal in the handset has to be shorted together in order to reduce the possibility of spurious resonance between different metallic layers. All the optimized parameters shown in Fig. 1 are tabulated in Table 1.

TABLE 1. Parameters of the proposed structure.

parameter	value (mm)	parameter	value (mm)
W	71	L_6	14.8
L	15.5	G	1.0
L_1	5.0	G_1	1.0
L_2	7.0	P_1	9.0
L_3	1.0	P_2	8.5
L_4	5.5	P_3	4.7
L_5	3.0	P_4	4.5

III. OPERATING MECHANISM

This section is going to illustrate the working principle of the proposed handset antenna elaborately. The performance evaluation software used in this work is CST Microwave Studio ®.

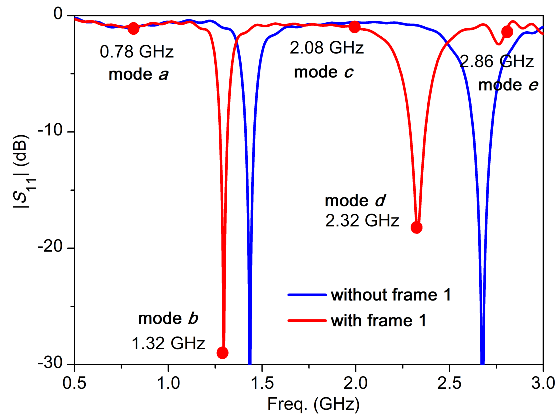

FIGURE 2. Simulated result of $|S_{11}|$ with and without frame 1.

A. THE EFFECT OF THE FRAME 1

The antenna structure with and without frame 1 are investigated and first compared to understand the function of frame 1. During the simulation process, the switches are omitted to eliminate their influence, giving an insightful analysis on the structure itself. Analytical results are shown in Fig. 2 and Fig. 3, from which one can observe that adding frame 1 is able to lower the resonant frequencies, in turn helping the antenna achieve more miniaturized size while enhancing the robustness of the handset simultaneously. The effect of the frame shown in Fig. 1(a) can be considered as a capacitive parallel loading to the radiating arms of the antenna. Hence, it is reasonable that the structure with frame 1 is able to achieve lower resonant frequency. Additionally, there are two obvious resonances (mode *b* and mode *d*) that can be seen in Fig. 2, even though there are five resonant modes existing below 3 GHz when observing the surface current distributions, as shown in Fig. 3. Here, only the modes under good impedance matching condition could be revealed in the reflection coefficient (S_{11}) result, for the S_{11} has a close relationship between the input impedance of each mode and the characteristic impedance of the feeding port.

B. POTENTIAL MODES OF THE ANTENNA

The five resonant modes could be identified approximately according to its current null point and peak point, as each mode's current amplitude vs. antenna's effective length could be characterized as a cosine curve. Note that the amplitude of the modes may not obey the cosine curve exactly. Nevertheless, the abovementioned approximation can easily help distinguish the different modes separately by its mode order along the main radiating arm. According to the approximation, mode *a* and mode *e* are generated by the longer arm (left side) of the metal-frame, where mode *e* is the third order of mode *a*, as illustrated in Fig. 3(f). Hence, mode *c* can be considered as the first order mode of the shorter arm (right side). Similarly, mode *b* and mode *d* are more likely generated from the first and second order modes of the whole metal-frame. When one part of the metal-frame works for a certain mode; the other parts of the metal-frame can be regarded as loadings

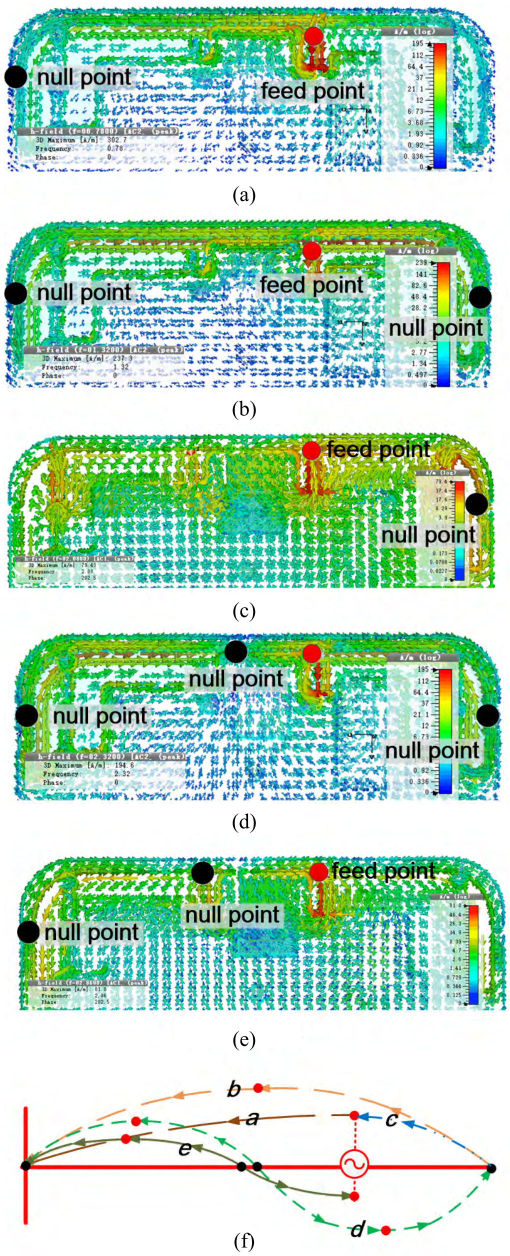

FIGURE 3. Simulated surface current at different frequencies: (a) at 860MHz; (b) at 1740MHz; (c) at 2080MHz; (d) at 2600MHz; (e) at 2860MHz; (f) surface current demonstrated approximately for all modes from (a) to (e).

to the main radiating arm. Therefore, the whole metal-frame has certain effect on each mode's radiation performance. However, modes *a*-*e* would be a better way to reveal the most relevant radiation parts at each resonant frequency, and would be useful for the mode control method (MCM) introduced by the switches.

C. MODE CONTROL METHOD INTRODUCED BY THE SWITCHES

From the mode analysis above, one can find that the proposed metal-frame handset structure has five potential radiating modes (below 3000 MHz), which can be utilized to cover

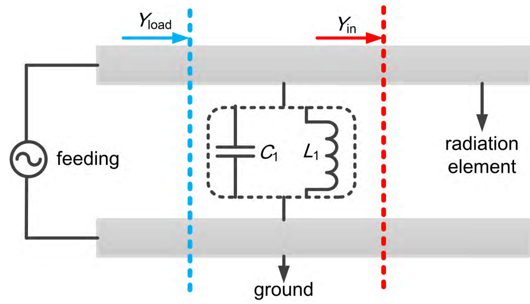

FIGURE 4. Equivalent circuit of antenna with L_1 or C_1 loading.

the desired LTE/WWAN bands, as long as it is possible to excite these modes. In this work, the application of the four switches is an efficient way to generate and control the five radiating modes, which is an embodiment of the abovementioned MCM proposed in this work.

1) LOADING SWITCHES FOR MCM

Analysis concerning the four switches and the MCM are elaborately discussed below. In Fig. 2, modes *a* and *b* are possible to be adjusted to generate the lower bands of LTE/WWAN (690 MHz-960 MHz). In addition, modes *c*, *d* and *e* could be used for the higher bands (1710 MHz-2690 MHz). However, only using the metal-frame as the antenna radiator cannot fully cover the desired bandwidths (690 MHz-960 MHz and 1710 MHz-2690 MHz) without the switches. Therefore, according to MCM, switches ①, ② ③ and ④ are introduced to control certain modes so as to achieve wideband characteristic. As aforementioned, switch ① can adjust the input impedance matching of the antenna, while switches ②, ③ and ④ act as parallel loadings to the antenna body at different locations. To make an intensive insight into the loading mechanism, two aspects of fact have to be studied theoretically. The first one is the relationship between the switches' location and their effect on the resonating frequency. The second one is how to ensure the values of each lumped element connected to the switches which would also be beneficial to enhance the antenna operating bandwidth.

2) SWITCHES' LOCATION AND LUMPED ELEMENTS

Fig. 4 presents the equivalent circuit of the antenna with parallel loading. The switches ②, ③ and ④ involved in the design together with the lumped elements connected to the ground act as parallel loadings for the metal-frame antenna. Hence, the following equations are established.

$$Y_{\text{load}} = Y_{\text{in}} + j\omega C_1 \tag{1}$$

$$K = \frac{Y_{\text{load}}}{Y_{\text{in}}} = 1 + \frac{j\omega C_1}{Y_{\text{in}}} \tag{2}$$

$$Y_{\text{load}} = Y_{\text{in}} + \frac{1}{j\omega L_1} \tag{3}$$

$$K = \frac{Y_{\text{load}}}{Y_{\text{in}}} = 1 + \frac{\frac{1}{j\omega L_1}}{Y_{\text{in}}} \tag{4}$$

Assuming that the input admittance without the loadings is represented by Y_{in}, and the one with the loadings is Y_{load}

(looking from the feed point to the loading location). The relationship between Y_{in} and Y_{load} is denoted in (1) and (4), where C_1 stands for capacitive loading and L_1 stands for inductive loading. The ratio K is used to evaluate the effect of the loading. According to (2) and (4), a smaller Y_{in} causes a more significant influence on the input admittance of the proposed antenna. In order to increase the sensitivity of the loading to the input admittance, the loading should be located at the place where Y_{in} reaches its minimum value both for the capacitive and inductive loading. From this point of view, appropriate locations of the switches can be determined via theoretical analysis and surface current simulation as aforementioned.

The loading influence on the shift of the radiating frequency should also be investigated. In the case of conventional resonating circuits, capacitance in parallel would result in a lower resonating frequency, while inductance in parallel has the opposite effect on the resonating frequency. Such theory can be easily transferred to the antenna loading in parallel. Furthermore, a larger value of capacitance or a smaller value of inductance would result in a more significant shift on the resonating frequency according to equations (2) and (4). Therefore, different lumped elements loaded to the switches can change the antenna resonating frequency, which in turn helps the antenna to achieve a wider working bandwidth according to MCM.

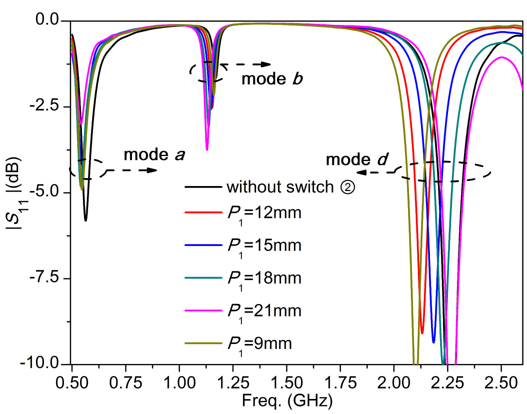

FIGURE 5. The relationship between the location of the switch ② and the shift of the radiation frequency. (Switch ①: 4 nH, switch ②: 0.6 Pf, switch ③: off, switch ④: 0.6 Pf).

3) VERIFICATION

To verify equations (1) to (4), one could take switch ② as an illustration. The relationship between the location of switch ② and the range of the frequency shift is presented in Fig. 5. Its corresponding surface current at certain frequency is shown in Fig. 6. Different locations of the loading may result in different ranges of frequency shift for a certain resonating mode. Besides, for different modes, the shifting range may also be different. The S_{11} without switch ② is illustrated in Fig. 5, and the three modes (mode *a*, mode *b* and mode *d*) are clearly shown on the curve. A 0.6 pF parallel loading is added to switch ②. Five curves with different P_1 values are presented compared with the one without switch ②. For modes *a* and *b*, switch ② is located at the location where the modes' currents get their relatively large value. According to equations (1)-(4), the loading introduced by switch ② can hardly change the resonating frequency of modes *a* and *b*, and its influence on the antenna performance will become smaller when switch ② moves to the USB component. Nevertheless, for mode *d*, the switch is located at the current null point and the frequency shift introduced by switch ② is quite obvious. When switch ② moves to the current null point, the shift range would also become larger, as observed from Fig. 5. Consequently, switch ② can be used to change the resonating frequency of mode *d*. The presented curves agree well with the corresponding theoretical predictions. Likewise, the other two switches ③ and ④ are also introduced to change other modes' resonating frequencies, and their locations are settled via both theoretical and simulation analysis. Their corresponding parameters P_1-P_4 are also listed in Table 1.

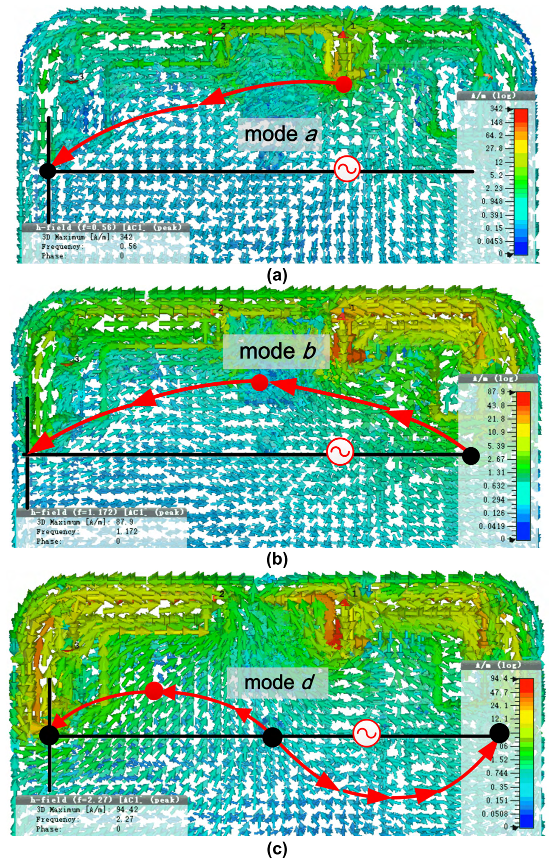

FIGURE 6. The simulated surface current for corresponding to Fig. 4 for the mode *a*, mode *b* and mode *d*; (a) for mode *a*; (b) for mode *b*; (c) for mode *d*.

4) MODES CONTROL REALIZATION IN ANTENNA

The four switches with different lumped elements are studied via simulation in order to demonstrate the MCM through the parallel loading introduced by the switches. Fig. 7 shows the influence exerted by switch ①. The switch is located along the feed point, acting as an adjustment stuff of the input impedance matching. When 4 nH is applied to the matching

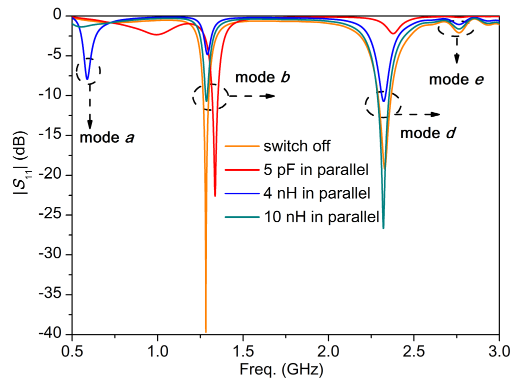

FIGURE 7. The simulated $|S_{11}|$ for switch ① with different lumped elements. (Switches ②, ③ and ④: off).

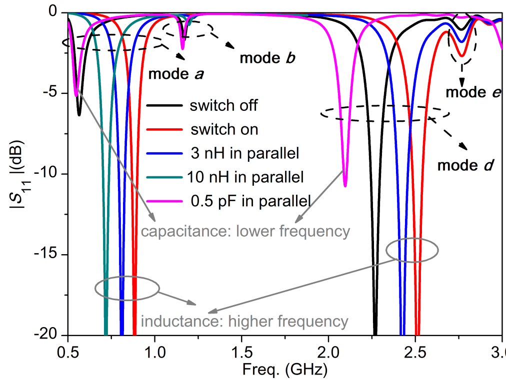

FIGURE 8. The simulated $|S_{11}|$ for switch ② with different lumped elements. (Switch ①: 4 nH, switch ③: off, switch ④: 0.6 Pf).

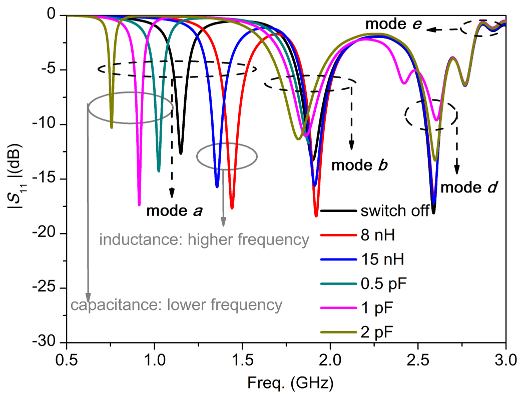

FIGURE 9. The simulated $|S_{11}|$ for switch ③ with different lumped elements. (Switch ①: off, switch ②: 0 Ω, switch ④: off).

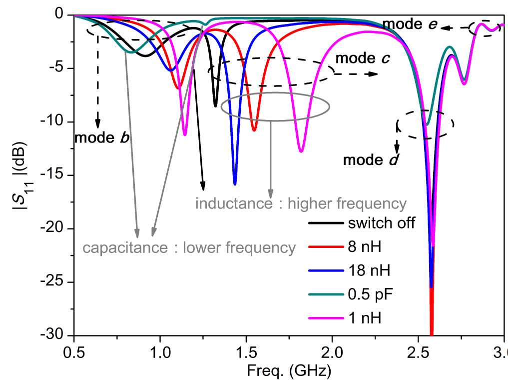

FIGURE 10. The simulated $|S_{11}|$ for switch ŕ with different lumped elements. (Switch ①: off, switch ②: 0 Ω, switch ③: off).

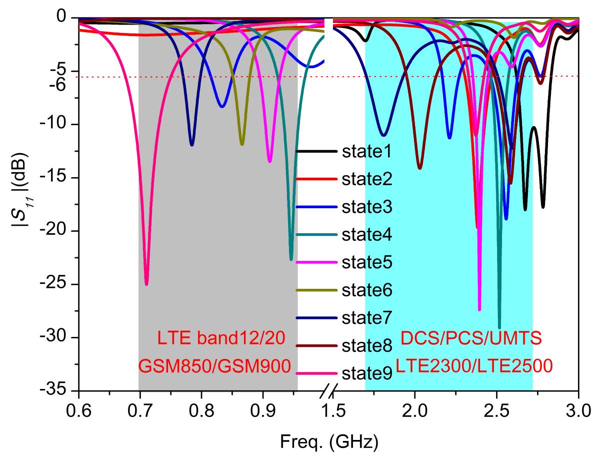

FIGURE 11. The simulated $|S_{11}|$ of the nine states to cover the desired bandwidth.

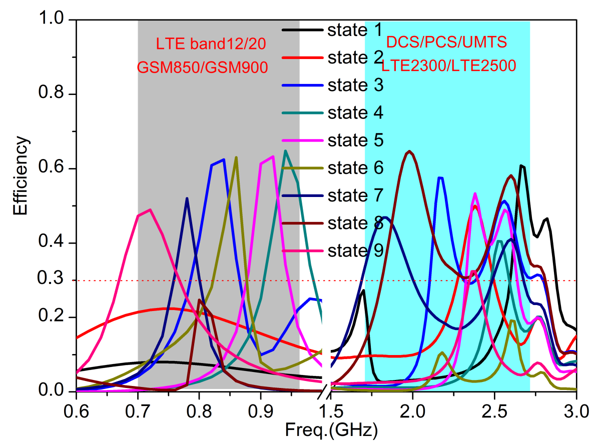

FIGURE 12. The simulated efficiency of the nine states to cover the desired bandwidth.

network, mode a can be generated, which can be utilized to cover the lower bands of the LTE/WWAN. In the same way, the effect of switch ② is demonstrated in Fig. 8. The switch would effectively shift the resonating frequency of mode d but has little effect on mode b and mode e, because the switch is located at the current null point of the mode d. As shown in Fig. 9, switch ③ is introduced to adjust mode a without any distinct influence on the other modes. Also, switch ④ will highly affect mode c as shown in Fig. 10.

According to Figs. 7-10, it can be observed that the capacitive loading induces a lower resonating frequency, whereas the inductive loading has an opposite effect. In addition, either a large value of capacitive element or a small value of inductive element results in a more significant shift compared with the original resonating frequency without the parallel loading.

After the above analysis on the switches and the loading effect, nine states of the proposed antenna are introduced

TABLE 2. Nine states of the proposed antenna.

	switch ①	switch ②	switch ③	switch ④
state 1	off	1.5 pF	off	off
state 2	off	18 nH	off	off
state 3	off	15 pF	off	0.6 pF
state 4	4 nH	15 pF	off	0.6 pF
state 5	4 nH	15 pF	1 pF	0.6 pF
state 6	5 pF	15 pF	1.8 pF	0.6 pF
state 7	off	0Ω	1.8 pF	0Ω
state 8	off	0Ω	1.8 pF	4 pF
state 9	4 nH	18 nH	off	off

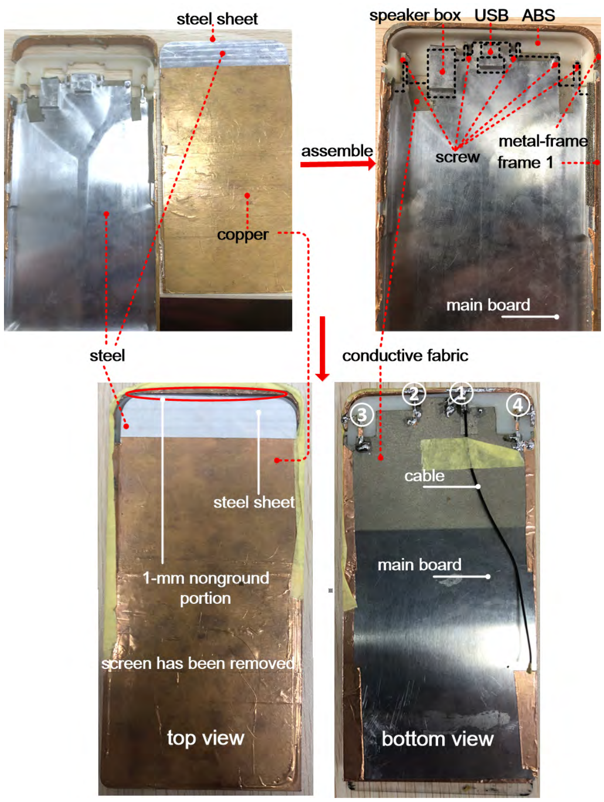

FIGURE 13. The photo of the proposed structure.

to achieve the desired operating bandwidth. The reflection coefficient and efficiency of the nine states are shown in Figs. 11 and 12, respectively. The nine states that correspond to the four switches are also summarized in Table 2.

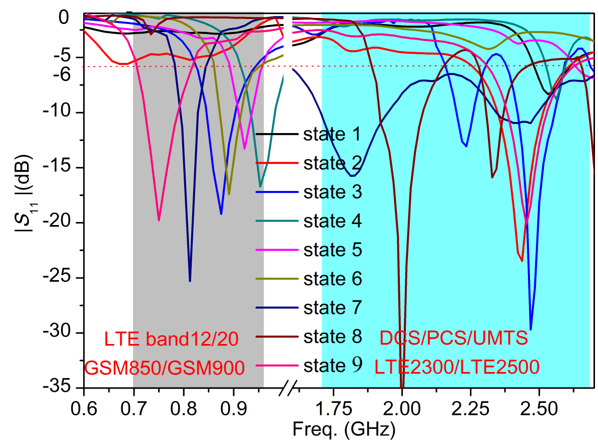

FIGURE 14. The measured $|S_{11}|$ of the nine states to cover the desired bandwidth.

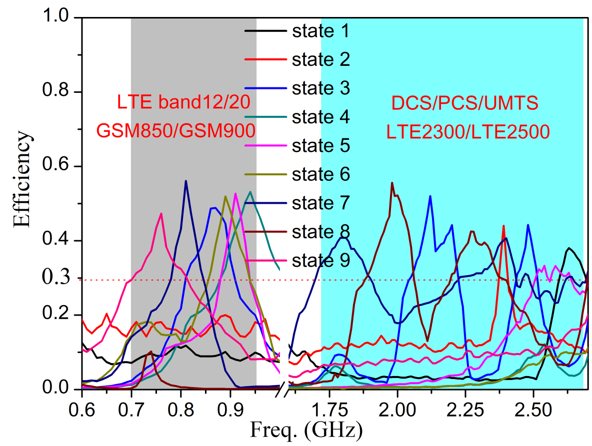

FIGURE 15. The measured efficiency of the nine states to cover the desired bandwidth.

TABLE 3. Nine states of the measured results.

	switch ①	switch ②	switch ③	switch ④
state 1	off	1.8 pF	off	off
state 2	off	18 nH	off	off
state 3	off	15 pF	off	0.5 pF
state 4	4.3 nH	15 pF	off	0.5 pF
state 5	4.3 nH	15 pF	1 pF	0.5 pF
state 6	4.7 pF	15 pF	1.8 pF	0.5 pF
state 7	off	0Ω	1.8 pF	0Ω
state 8	off	0Ω	1.8 pF	3.9 pF
state 9	4.3 nH	18 nH	off	off

IV. MEASURED RESULTS AND DISCUSSION

A prototype was fabricated to verify the design performance, as shown in Fig. 13. The measured reflection coefficient and efficiency of the prototype antenna are shown in Figs. 14 and 15, respectively. In order to cover the desired bandwidth, the nine states are all measured by soldering different lumped elements at the four locations (namely, ①, ②, ③ and ④). It should be emphasized that the lumped elements are used instead of the four practical switches to verify the mode control principle. Minor disagreement between the simulated model and the prototype results are demonstrated between Table 2 and the Table 3. Finally, wideband characteristic can be attained within the 699 MHz-960 MHz band (for Bands 1, 2, 5, 8, 12 and 20) and 1710 MHz-2690 MHz band (for UMTS, DCS, PCS and LTE bands) with S_{11} < -6 dB. Furthermore, the radiation efficiencies measured across the desired bands were between 30% and 55%. According to practical engineering requirements and applications, the radiation performances of the proposed antenna are satisfactory, because good user experience can be obtained as long as the antenna achieves an efficiency of more than 30%.

V. CONCLUSION

A frequency-reconfigurable antenna with 1-mm nonground portion for metal-frame and full-display screen handset applications is proposed. Four switches are introduced to control certain resonating modes so as to cover the bandwidth of 699 MHz-960 MHz and 1710 MHz-2690 MHz. The efficiency for the proposed antenna is as high as 55%, which is sufficient to meet majority of practical requirements for handset antenna applications. The utilization of the switches overcomes severe internal hardware environment introduced by the 1-mm nonground portion and other surrounding metallic components such as USB, steel sheet and speaker box. The mode control method introduced by the switches can effectively enhance the operating bandwidth of the proposed antenna.

REFERENCES

[1] C. Rowell and E. Y. Lam, "Mobile-phone antenna design," *IEEE Antennas Propag. Mag.*, vol. 54, no. 4, pp. 14–34, Aug. 2012.

[2] R. Tang and Z. Du, "Wideband monopole without lumped elements for octa-band narrow-frame LTE smartphone," *IEEE Antennas Wireless Propag. Lett.*, vol. 16, pp. 720–723, 2016.

[3] K.-L. Wong and C.-Y. Tsai, "IFA-based metal-frame antenna without ground clearance for the LTE/WWAN operation in the metal-casing tablet computer," *IEEE Trans. Antennas Propag.*, vol. 64, no. 1, pp. 53–60, Jan. 2016.

[4] M. Zheng, H. Wang, and Y. Hao, "Internal hexa-band folded monopole/dipole/loop antenna with four resonances for mobile device," *IEEE Trans. Antennas Propag.*, vol. 60, no. 6, pp. 2880–2885, Jun. 2012.

[5] K.-L. Wong and Y.-C. Chen, "Small-size hybrid loop/open-slot antenna for the LTE smartphone," *IEEE Trans. Antennas Propag.*, vol. 63, no. 12, pp. 5837–5841, Dec. 2015.

[6] L.-W. Zhang, Y.-L. Ban, C.-Y.-D. Sim, J. Guo, and Z.-F. Yu, "Parallel dual-loop antenna for WWAN/LTE metal-rimmed smartphone," *IEEE Trans. Antennas Propag.*, vol. 66, no. 3, pp. 1217–1226, Mar. 2018.

[7] D. Huang and Z. Du, "Eight-band antenna with a small ground clearance for LTE metal-frame mobile phone applications," *IEEE Antennas Wireless Propag. Lett.*, vol. 17, no. 1, pp. 34–37, Jan. 2018.

[8] H. Chen and A. Zhao, "LTE antenna design for mobile phone with metal frame," *IEEE Antennas Wireless Propag. Lett.*, vol. 15, pp. 1462–1465, 2015.

[9] Y. Liu, Y. Luo, and S. Gong, "An antenna with a stair-like ground branch for Octa-band narrow-frame mobile phone," *IEEE Antennas Wireless Propag. Lett.*, vol. 17, no. 8, pp. 1542–1546, Aug. 2018.

[10] H.-B. Zhang, Y.-L. Ban, Y.-F. Qiang, J. Guo, and Z.-F. Yu, "Reconfigurable loop antenna with two parasitic grounded strips for WWAN/LTE unbroken-metal-rimmed smartphones," *IEEE Access*, vol. 5, pp. 4853–4858, 2017.

[11] Y. Liu, Y.-M. Zhou, G.-F. Liu, and S.-X. Gong, "Heptaband inverted-F antenna for metal-rimmed mobile phone applications," *IEEE Antennas Wireless Propag. Lett.*, vol. 15, pp. 996–999, 2015.

[12] H. Xu *et al.*, "A compact and low-profile loop antenna with six resonant modes for LTE smartphone," *IEEE Trans. Antennas Propag.*, vol. 64, no. 9, pp. 3743–3751, Sep. 2016.

[13] Y. K. Park and Y. Sung, "A reconfigurable antenna for quad-band mobile handset applications," *IEEE Trans. Antennas Propag.*, vol. 60, no. 6, pp. 3003–3006, Jun. 2012.

[14] M. Stanley, Y. Huang, H. Wang, H. Zhou, Z. Tian, and Q. Xu, "A novel reconfigurable metal rim integrated open slot antenna for octa-band smartphone applications," *IEEE Trans. Antennas Propag.*, vol. 65, no. 7, pp. 3352–3363, Jul. 2017.

[15] K. Yan, P. Yang, F. Yang, and S. Y. Huang, "Antenna design for a smartphone with a full metal casing and a narrow frame," *IET Microw. Antennas Propag.*, vol. 12, no. 8, pp. 1316–1323, Jul. 2018.

[16] L. Qu, J. Jeon, D. Park, and H. Kim, "Antenna design based on quasi-degenerate characteristic modes of unbroken metal rim," *IET Microw. Antennas Propag.*, vol. 11, no. 15, pp. 2168–2173, Dec. 2017.

[17] S.-C. Chen, C.-C. Huang, and W.-S. Cai, "Integration of a low-profile, long-term evolution/wireless wide area network monopole antenna into the metal frame of tablet computers," *IEEE Trans. Antennas Propag.*, vol. 65, no. 7, pp. 3726–3731, Jul. 2017.

[18] Y. Yang, Z. Zhao, W. Yang, Z. Nie, and Q.-H. Liu, "Compact multimode monopole antenna for metal-rimmed mobile phones," *IEEE Trans. Antennas Propag.*, vol. 65, no. 5, pp. 2297–2304, May 2017.

[19] C.-Z. Han, G.-L. Huang, T. Yuan, W. Hong, and C.-Y.-D. Sim "A frequency-reconfigurable tuner-loaded coupled-fed frame-antenna for All-metal-shell handsets," *IEEE Access*, vol. 6, pp. 64041–64049, 2018.

CHONG-ZHI HAN received the B.E. and M.E. degrees in electronic information engineering from the Harbin Institute of Technology, Harbin, China. He is currently pursuing the Ph.D. degree in information and communication engineering with Shenzhen University, Shenzhen, China. His current research interests include the development and application of MIMO terminal antennas, and millimeter wave antenna.

SHU-MIN LIAO received the B.E. degree from Hubei Normal University, Hubei, China. She is currently pursuing the master's degree in information and communication engineering with Shenzhen University, Shenzhen, China. Her current research interest includes the development and application of mobile terminal antennas.

KAI-DONG HONG received the B.E. degree in communication engineering from Guangdong Ocean University, Guangdong, China. He is currently pursuing the Ph.D. degree in information and communication engineering with Shenzhen University, Shenzhen, China. His current research interests include the planar antennas and millimeter wave antennas.

GUAN-LONG HUANG (M'11–SM'18) received the B.E. degree in electronic information engineering from the Harbin Institute of Technology, Harbin, China, and the Ph.D. degree in electrical and computer engineering from the National University of Singapore, Singapore.

He was with the Nokia Solutions and Networks System Technology as a Senior Antenna Specialist, from 2011 to 2017. He has been with the Temasek Laboratories, National University of Singapore, as a Research Scientist. He is currently an Assistant Professor with the College of Information Engineering, Shenzhen University, Shenzhen, Guangdong, China. He also serves as the Deputy Director of the Guangdong Provincial Mobile Terminal Microwave and Millimeter-Wave Antenna Engineering Research Center. He has authored or coauthored more than 100 papers in journals and conferences. His research interests include the design and implementation of planar antenna arrays, 5G base-station and mobile RF front-end devices/antennas, phased antenna arrays, channel coding for massive MIMO applications, and 3-D printing technology in microwave applications. He is currently serving as an Associate Editor for the IEEE ACCESS.

TAO YUAN received the bachelor's and master's degrees from Xidian University, China, and the Ph.D. degree from the National University of Singapore, Singapore. He is currently a Professor with the College of Information Engineering, Shenzhen University, Shenzhen, China. His current research interests include developing novel RF modules and antennas for mobile terminal, and 5G applications.

WONBIN HONG (S'04–M'09–SM'14) received the B.S. degree in electrical engineering from Purdue University, West Lafayette, IN, USA, in 2004, and the master's and Ph.D. degrees in electrical engineering from the University of Michigan, Ann Arbor, MI, USA, in 2005 and 2009, respectively.

From 2009 to 2016, he was with Samsung Electronics, Suwon, South Korea, as a Principal and Senior Engineer, participating and leading extensive research and development tasks for upcoming wireless applications, including MIMO, wireless power transfer, and millimeter-wave wireless solutions. He is currently with the Department of Electrical Engineering, Pohang University of Science and Technology, Pohang, South Korea, as an Assistant Professor. He has well over a decade of extensive research and development experience with primary interest in future wireless communication antennas and RF circuits, mesoscale and nanoscale transparent electronics, and 3-D packaging. He has authored and coauthored over 80 peer-reviewed journals, conference papers, and two book chapters, and is an inventor of over 80 patent inventions. He is a member of the Technical Committee of the IEEE MTT-6 Microwave and Millimeter-Wave Integrated Circuits. He was a recipient of numerous recognitions, including the Outstanding Researcher of the Year Award, the Outstanding Mentor of the Year Award, the Major Achievement Award, the Annual Inventor Award, and the Samsung Best Paper Award during his tenure at Samsung. Owing to his accomplishments, he was promoted to the rank of Principal Engineer within the shortest period in the history of the Business Division, Samsung. He was also awarded several fellowships and scholarships, including the Samsung Scholarship Award for Graduate Studies, the Rappaport Wireless Scholarship, the NASA Summer Undergraduate Research Fellowship, the A.F. Welch Scholarship, and the Donald McQuinn Scholarship. His students have received the 2018 Outstanding Master's Student Award, Electrical Engineering Department, POSTECH, the Silver Medal in the 14th Samsung Electro-Mechanics Best Paper Award, the 1st Prize Best Student Paper Award in the 2018 IEEE ISAP, and the Best Paper Award in the 2017 ISMOT. He has served as an Invited Lecturer and a Speaker in over 80 international research symposiums and government and industry sessions held around the world. He is currently serving as an Associate Editor for the IEEE TRANSACTION ON ANTENNAS AND PROPAGATION and a Guest Editor of the IEEE ANTENNAS AND WIRELESS PROPAGATION LETTERS Special Cluster on Antenna-in-Package, Antenna-on-Chip, Antenna-IC Interface: Joint Design and Co-Integration. From 2016 to 2017, he was a Guest Editor of the IEEE TRANSACTION ON ANTENNAS AND PROPAGATION Special Edition on Antennas and Propagation Aspects of 5G Communications.

CHOW-YEN-DESMOND SIM (M'07–SM'13) was born in Singapore, in 1971. He received the B.Sc. degree from the Engineering Department, University of Leicester, U.K., in 1998, and the Ph.D. degree from the Radio System Group, Engineering Department, University of Leicester, in 2003. From 2003 to 2007, he was an Assistant Professor with the Department of Computer and Communication Engineering, Chienkuo Technology University, Changhua, Taiwan. In 2007, he joined the Department of Electrical Engineering, Feng Chia University (FCU), Taichung, Taiwan, as an Associate Professor, where he became a Full Professor, in 2012, and as a Distinguish Professor, in 2017. He has served as the Executive Officer of the Master's Program at the College of Information and Electrical Engineering (Industrial Research and Development) and the Director of the Intelligent IoT Industrial Ph.D. Program, from 2015 to 2018. He is currently serving as the Head of the Department of Electrical Engineering and the Director of the Antennas and Microwave Circuits Innovation Research Center, FCU. He has authored or coauthored over 120 SCI papers. His current research interests include antenna design, VHF/UHF tropospheric propagation, and RFID applications. He is a Fellow of the Institute of Engineering and Technology (FIET), a Senior Member of the IEEE Antennas and Propagation Society, and a Life Member of the IAET. He served as the TPC Member of the APMC 2012, the APCAP 2015, IMWS-Bio 2015, CSQRWC 2016, ICCEM 2017, APCAP 2018, and CIAP 2018. He was a recipient of the IEEE Antennas and Propagation Society Top Ten Outstanding Reviewer Award (the IEEE TRANSACTION ANTENNAS AND PROPAGATION) for periods 2013/2014, 2014/2015, 2015/2016, 2016/2017, and 2017/2018. He has also served as the TPC Sub-Committee Chair (Antenna) of the ISAP 2014 and the PIERS 2017. He was invited as the Workshop/Tutorial Speaker in APEMC 2015, iAIM 2017, INCAP 2018, and an Invited Speaker of TDAT 2015, iWAT 2018, and APCAP 2018. He was the Keynote Speaker of SOLI 2018. He served on the Advisory Committee of InCAP 2018. He has served as the TPC Chair of the APCAP 2016 and the Chapter Chair of the IEEE AP-Society, Taipei Chapter (from 2016 to 2017). He has been the Founding Chapter Chair of the IEEE Council of RFID, Taipei Chapter (since 2017). He is currently serving as the Associate Editor of the IEEE AWPL, the IEEE ACCESS, the IEEE JRFID, and the *International Journal of RF and Microwave Computer-Aided Engineering* (Wiley). Since 2016, he has been serving as the Technical Consultant of Securitag Assembly Group (SAG), which is one of the largest RFID tag manufacturers in Taiwan. He has also received the Outstanding Associate Editor Award from the IEEE ANTENNAS WIRELESS AND PROPAGATION LETTERS, in 2018.